

Toward Enabling Spatial Control of Ti-6Al-4V Solidification Microstructure in the Electron Beam Melting Process

Sneha P. Narra¹, Ross Cunningham², Daniel Christiansen¹, Jack Beuth¹ and Anthony D. Rollett²

¹Department of Mechanical Engineering, Carnegie Mellon Univ., Pittsburgh, PA 15213

²Material Science and Engineering Department, Carnegie Mellon Univ., Pittsburgh, PA 15213

Abstract

In this work, relationships between prior beta grain size in solidified Ti-6Al-4V and melting process parameters in the Arcam Electron Beam Melting (EBM) process are investigated. Toward this goal, samples are built on an Arcam S12 machine at Carnegie Mellon University by specifically varying the Arcam proprietary speed function and beam current over process space for a variety of test specimens. Optical microscopy is used to measure the prior beta grain widths and assess the number of prior beta grains present in a melt pool in the raster region of the build. Results demonstrate that the number of grains across the width of a bead is constant for a fixed deposition geometry. The resulting understanding of the relationship between primary machine variables and prior beta grain widths is a key step toward understanding and enabling the spatial control of as-built microstructure in the EBM process.

Introduction

Electron beam powder bed Additive Manufacturing (AM) is attractive due to its working conditions, e.g. elevated build temperature and a vacuum build environment, which help manufacture residual-stress-free and contamination-free components [1]. In addition, high beam powers and efficient transfer of power into the part yield high deposition rates and facilitate building of components from materials with high melting points up to 3500°C [2]. In this work Ti-6Al-4V (Ti64) is the material of interest owing to its extensive applications in the aerospace industry and also the availability of well-established control themes on the Arcam Electron Beam Melting (EBM) machine [1].

It is critical to know the mechanical behavior of AM as-built components to qualify them for use in industrial applications. This motivates this study of the effect of process variables on Ti64 solidification microstructure, which governs some mechanical properties of the end part [3]. At the same time, it is important to maintain or improve other process outcomes such as process precision and build rate, which are governed directly or indirectly by melt pool geometry. Hence, it is important to understand the integrated control of melt pool geometry and solidification microstructure. Toward this goal, techniques have been developed for integrated control of melt pool geometry and microstructure of Ti64 in an Electron Beam Wire Feed Process (EBF3) and in EBM for single bead geometries [4] [5]. Using these concepts of prior beta grain width control shown in Figure 1, in this work, beta grain width is varied by controlling the melt pool geometry using the primary beam parameters in the EBM process. Other previous work has explored the microstructure in Ti64 EBM deposits by describing the evolution of microstructure, mechanical properties and their dependence on part dimensions, build orientation, and location [6] [7] [8]. This

work focuses primarily on prior beta grain width control as a first step toward enabling full microstructure control in fabricated components using EBM machine process parameters. To the knowledge of the authors, this work is unique and it allows any EBM user with basic (Level 1) machine training to control prior beta grain widths in the raster regions of bulky as-built parts.

Microstructure generally affects mechanical properties and, unlike the alpha lath microstructure, it is difficult to modify as-built prior beta grain size through post-processing heat treatments [9] [10]. Prior beta grain size is mainly controlled by the rate at which the melt pool cools down from the melting temperature to the beta transus temperature during the process. This scales with the thermal conditions at the start of solidification, that is, the thermal gradient and resulting cooling rate at the solidus temperature, which in turn varies with the primary process parameters i.e. beam current and travel speed [11].

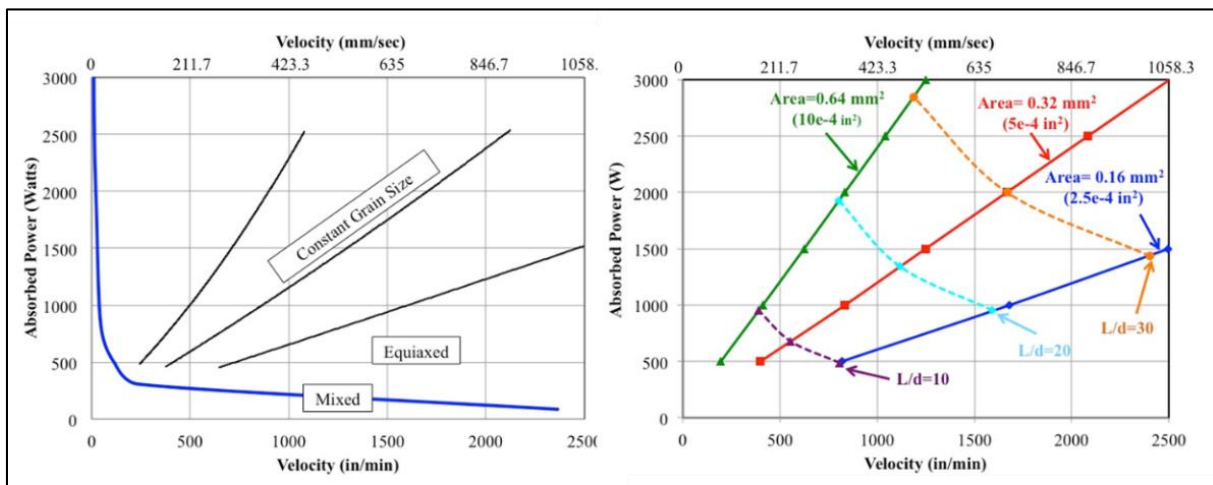


Figure 1: Plots showing integrated solidification microstructure and melt pool geometry control for Ti64 single beads during the electron beam melting process [5].

Arcam Electron Beam Melting Process

Primary variables for beam control in the EBM process are beam speed, beam current, and focus offset as shown in Figure 2. When a part is built in the automatic mode, beam current is changed with part height based on a thermal model in the machine's control software and speed is controlled by the variable speed function. Focus offset controls the spot size of the electron beam. In this work, the effect of focus offset is not discussed in detail and it is not methodically varied across its operating range. Focus offset is not expected to have a significant effect on beta grain size. The speed function is a proprietary variable and an initial study was performed to understand the role of this variable during the melting process. Mahale [12] discussed the variation of beam current and travel speed with part height for various speed function and layer thickness values. Using that data, lines of constant speed function (Figure 3) have been developed in power and velocity space.

Qualitative analysis of the data plotted in Figure 3 shows that curves of constant speed function have a similar trend to curves of constant melt pool area in Figure 1 from the previous work [5] [13] done on single bead tests in the Arcam EBM process. Therefore, we can say that, based on

the beam current, the speed function changes beam travel velocity in an attempt to maintain constant melt pool geometry throughout the build process. As a part of this work, experiments have been performed to establish a quantitative relationship between speed function and melt pool geometry which was then used to understand and control the prior beta grain width in solid blocks.

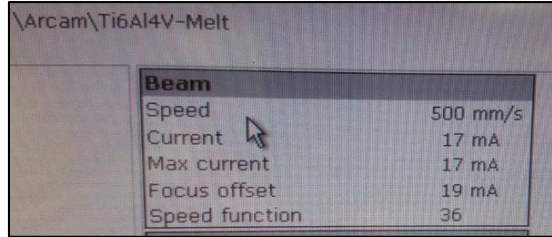


Figure 2: Photograph showing the primary beam variables on the Arcam machine.

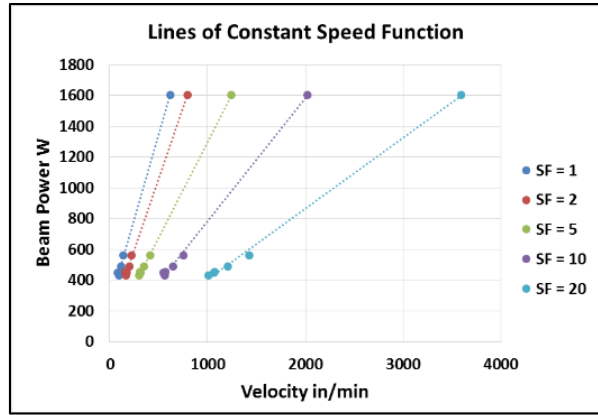


Figure 3: Plot demonstrating the effect of beam current and velocity (speed function).

Experimental Setup

Single Bead Tests

No-added-powder single bead tests have been performed for different speed function and beam current combinations as listed in Table 1 on an Arcam S12 machine at Carnegie Mellon University. In these tests, there was no powder on the Ti64 plate. The beam carrying a specified current and operating at a given speed function traveled from one end of the plate to the other leaving rectangular melt tracks as shown in Figure 4. The plate base was maintained at a temperature of approximately 750C.



Figure 4: Image of the Ti64 plate with single bead melt tracks.

Table 1: Parameter set used for the no-added-powder single bead experiments.

Sample No.	Beam Current mA	Speed Function	Focus Offset mA
1 (Nominal)	17	36	19
2	17	17	19
3	17	7	19
4	17	75	19
5	17	154	19
6	8.5	36	19
7	8.5	17	19
8	34	36	19
9	34	17	19
10	12	30	0
11	12	13	0
12	12	4	0
13	12	64	0
14	12	130	0
15	6	30	0
16	6	13	0
17	24	30	0
18	24	13	0

Multi-Layer Blocks (or Solid Builds)

Figure 5 shows the experimental layout of 9 multi-layer blocks of dimensions 30W×30L×20H mm built by varying speed function and beam current in the build theme (shown in Figure 6) while holding other melting parameters constant. This was done for both contour and bulk raster regions, though results are presented only for bulk raster regions in this study. From Table 2, it can be seen that out of 9 samples, 5 samples were built with varying speed function at a constant beam current. The remaining 4 samples were built with varying beam current at constant speed function. Sample 1 was built using nominal build conditions for the Ti64 alloy.

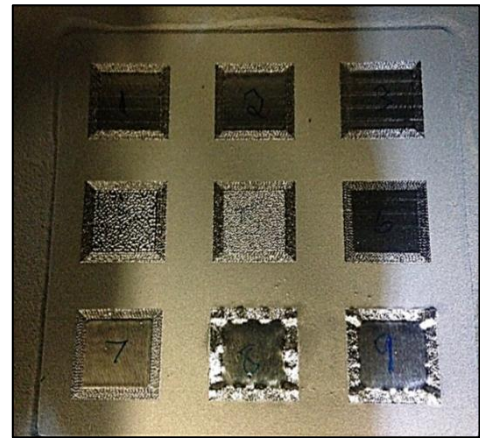


Figure 5: Layout for multi-layer block experiments.

Experimental Results and Analysis

Single Bead Tests

Single bead melt lines were sectioned along the transverse direction of the melt track at locations well away from the plate edges, where the melt pool reaches steady-state conditions. Samples were mounted, polished and etched using Kroll's reagent [4]. Images were taken using an Alicona InfiniteFocus optical microscope.

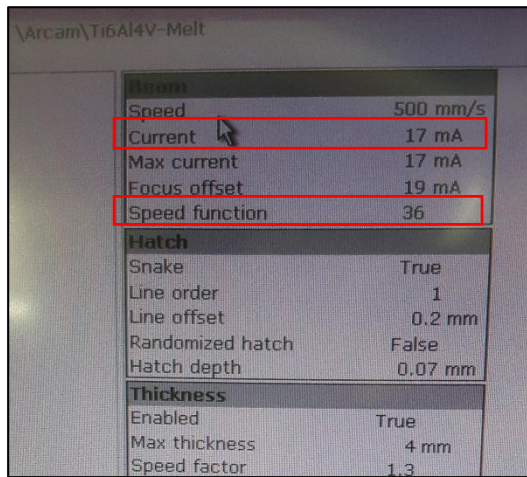


Figure 6: Image showing various parameters on the machine that control the melting process.

Table 2: Parameters for multi-layer block experiments.

Block No.	Beam Current mA	Speed Function
1 (Nominal)	17	36
2	17	17
3	17	7
4	17	75
5	17	154
6	8.5	36
7	8.5	17
8	34	36
9	34	17

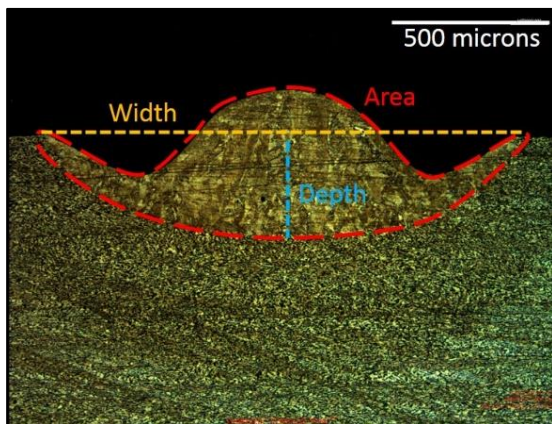


Figure 7: Example single bead melt pool cross-section with melt pool dimensions noted.

An example of a melt pool cross-section image used for analysis is shown in Figure 7. The melt pool is marked along the solidification boundary, which is where the morphology is different from the start plate. The melt pool dimensions of cross-sectional area, width and depth were measured. Grains grew from the melt pool boundary upward and toward the center and, qualitatively, a majority of the grains appear to be columnar. Samples 4, 5 and 8 had melt pools that were very shallow and made it difficult to mark the boundaries. Therefore, these samples were not considered in further analyses. Using the line intercept method [14], average prior beta grain size was measured from all the cross-sections.

A relationship between melt pool cross-sectional area and speed function was developed from analysis of the single bead tests. It follows a power law relationship, as illustrated in Figure 8. It is evident from the plot in Figure 8 that depending on the speed function, for a certain beam current, beam travel speed changes to maintain a constant melt pool cross-sectional area. An effective melt pool width has been calculated from the melt pool area by assuming the melt pool to be semi-circular where the diameter of the semi-circle is the effective width of the melt pool. This quantity was used in this study instead of the actual melt pool width to reduce the variability seen in actual melt pool widths and to ultimately relate beta grain widths to melt pool cross-sectional areas. The melt pool cross sectional area, A , is a key quantity, in that the melt rate is equal to the beam travel speed multiplied by A . To this end, it was also found that prior beta grain width scales with effective width as shown in Table 3 and Figure 9. The number of grains per effective melt pool width is approximately 20 (the slope of the line in Figure 9).

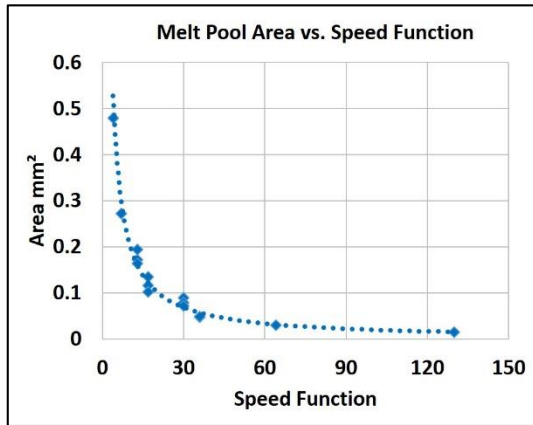


Figure 8: Plot demonstrating the relationship between melt pool cross-sections and speed function.

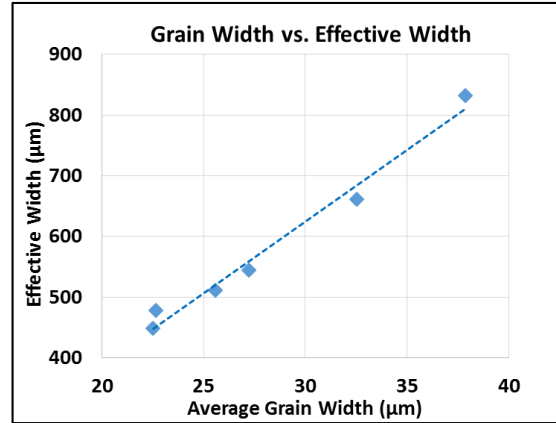


Figure 9: Illustration of average grain width scaling with effective melt pool width for single beads.

In previous work [5], Gockel found that melt pool grain size scales with effective melt pool effective width for single beads in the Arcam process. In that work, the author conducted experiments by directly varying power and velocity to maintain a constant cross-sectional area of the melt pool. In this work, velocity is not controlled explicitly by the user, but the machine parameter speed function is changed to vary the velocity to yield a melt pool with constant cross-section area. Both studies show that prior beta grain width scales with effective melt pool width. An important contribution of this study is the extension of this concept from single bead geometries to solid builds to determine if the relationship between effective melt pool width and prior beta grain width still holds true. This issue is considered in the next section.

Table 3: Measurements of average prior beta grain widths for single beads.

Sample No.	Beam Current (mA)	Speed Function	Melt Pool Area (mm ²)	Avg. Prior Beta Grain Width (μm)	Effective Width (μm)	Effective Width/Grain Width
2	17	17	0.12	27	545	20
3	17	7	0.27	38	832	22
7	8.5	17	0.10	26	512	20
11	12	13	0.17	33	661	20
15	6	30	0.08	23	448	20
10	12	30	0.09	23	478	21

Multi-Layer Blocks (or Solid Builds)

Multi-Layer blocks were vertically sectioned at the center, mounted, polished and etched using Kroll's reagent. Images were taken with a 20X objective using a Zeiss Light Optical Microscope. Dark field mode was used to increase the contrast of boundary alpha phase, which aids in identifying the prior beta grains, and phase colors were reversed to identify the grain boundary alpha clearly.

It was observed that the solid build microstructure consists of columnar grains growing along the build height. This has been reported in previous work focusing on understanding Ti64 solidification microstructure. There were no traces of individual melt pools or powder layers in the final build as the grains grow through layers. This can be due to remelting caused by the pre-heating step and heat from melting subsequent layers during the build process [6] [7]. Figure 10 shows microstructure resulting from the nominal parameters on the machine, at a magnification level chosen to show multiple prior beta grains.

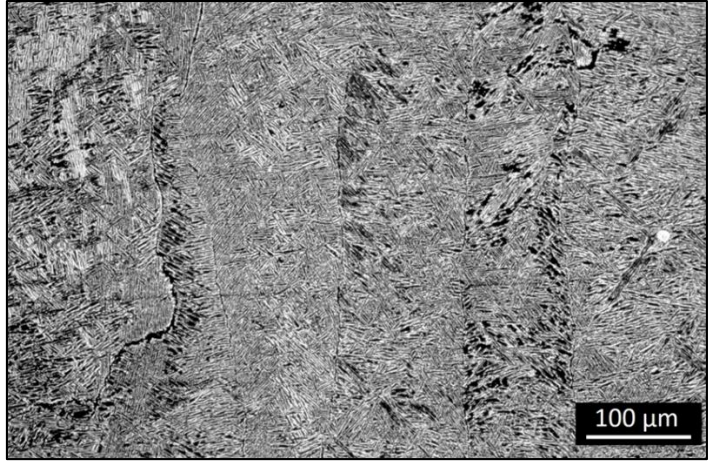


Figure 10: Cross-section image of the block built with nominal parameters on an Arcam S12 machine at Carnegie Mellon University.

Grain widths were measured from the blocks using the line intercept method [14] at the heights of 19 mm, 17 mm, 15 mm, and 12.5 mm across the bulk raster region as illustrated in Figure 11. At the part heights considered, there is a large variation in grain widths across the width of the sample. However, the variability of the average grain widths across all heights in a single test block is low. Table 4 summarizes the average prior beta grain widths across height for different test blocks. In this analysis, blocks 7 and 8 are saved for further analysis since blocks 6 and 9 address the case where beam current is being varied, but speed function is the same as in samples 1 and 2.

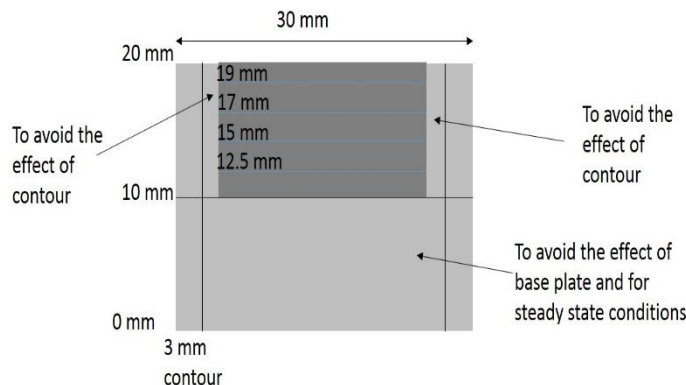


Figure 11: Illustration of the region considered for average prior beta grain width measurements.

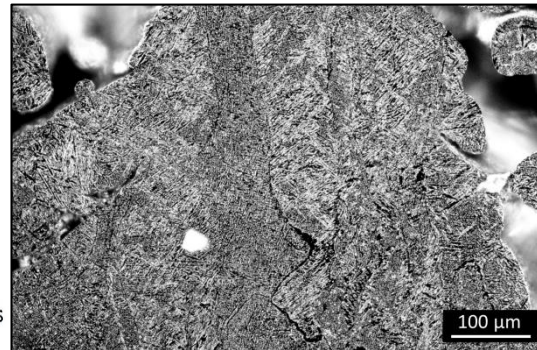


Figure 12: Cross-section image showing the microstructure of the block built with decreased grain size and smaller melt pools that resulted in porosity.

In all the samples, the grain growth pattern is similar to that observed in nominal case, with the exception of samples built with higher speed functions, yielding shallower melt pools. These specimens experienced significant porosity as shown in Figure 12. In these cases, heat transfer pathways are different from that of fully melted samples, which leads to irregular microstructure

close to these pores compared to the completely melted cases. Measurements in these samples were taken in regions well away from the pores and their effects on microstructure.

Table 4: Average prior beta grain width measurements for multi-layer blocks.

Block No.	Beam Current (mA)	Speed Function	Avg. Grain Width (μm)
1 (Nominal)	17	36	124
2	17	17	186
3	17	7	271
4	17	75	91
5	17	154	69
6	8.5	36	120
9	34	17	185

It was also observed that irrespective of beam current, if the speed function is constant, prior beta grain size is constant. From single bead tests, it was observed that the speed function maintains a constant cross-sectional area that results in constant effective melt pool width. Hence it can be concluded that prior beta grain width scales with effective melt pool width for multi-layer blocks as evident from the plot in Figure 13.

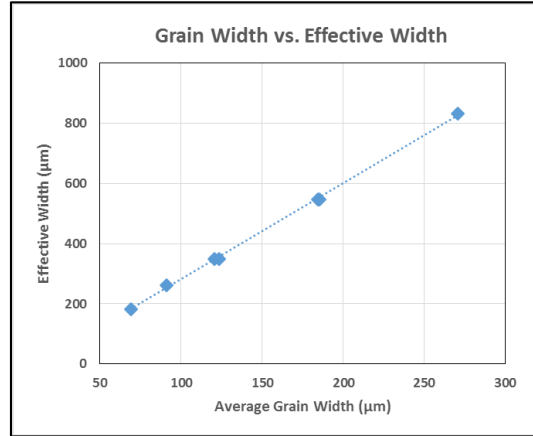


Figure 13: Illustration of average grain width scaling with effective melt pool width for multi-layer blocks.

Unlike the single bead experiment results, where the number of prior beta grains per effective melt pool width is 20-22, in the multi-layer blocks there were approximately 3 grains per effective melt pool width. This can be explained by the fact that in multilayer builds, columnar prior beta grains span multiple layers of the build and increase in width as they take the place of some grains that narrow and die out. In this study, the region of the solid builds where beta grain sizes were measured was in the top half of each block, where it was expected that a steady-state value of beta grain widths might exist. The lack of an observed variation in beta grain width indicates that steady-state conditions were achieved. It is expected that within the bottom 5mm of each block, a transition occurred between the small beta grain widths seen in the single bead tests to the much larger widths observed in this study. This is the subject of continuing work by the authors.

What is most interesting is that despite the complicated evolution of beta grain sizes in the multi-layer blocks, beta grain widths still scale with melt pool widths. This highlights the controlling role of solidification cooling rate (which scales with melt pool cross sectional area) and yields an important insight into how to control beta grain widths in raster builds of bulky parts. Control of melt pool cross sectional area (and the related effective melt pool width) results in the control of beta grain width.

Conclusions

Part qualification is critical for widespread commercialization of AM and knowledge about as-built properties is critical in speeding up the qualification process. This study contributes toward understanding and controlling as-built microstructure in the Arcam EBM process space, which in turn governs the mechanical properties of the as-built part.

The role of Arcam-defined beam parameters in controlling melt pool geometry and microstructure and also the principles of the Arcam machine control software have been determined in detail through literature review and experimentation. Based on the concept of prior beta grain width scaling with melt pool width for single-bead geometries for the Arcam EBM process and an electron beam wire feed process, prior beta grain width control has been extended to multi-layer blocks, i.e. multi-layer solid build geometries filled by raster patterns. Results demonstrate that prior beta grain width scales with effective melt pool width in solid builds. This greatly simplifies the strategy for controlling beta grain widths to one of controlling melt pool size. Further, this integrated melt pool dimension and microstructure control strategy is demonstrated to be achievable by modifying Arcam-defined beam variables that are accessible for any user with basic (Level 1) operational training.

Acknowledgements

The authors wish to acknowledge collaborations with Ronald Aman of the Rochester Institute of Technology, Timothy Horn of the North Carolina State University, and Frank Medina of Arcam AB for their valuable insights from their extensive experience using the Arcam EBM system. This research was supported by the National Science Foundation under grant CMMI 1335298.

References

- [1] Arcam, "Technology," [Online]. Available: <http://www.arcam.com/technology/electron-beam-melting/>. [Accessed 24 August 2015].
- [2] 3D Printing Systems, "Additive Manufacturing using metals," [Online]. Available: <http://3dprintingsystems.com/additive-manufacturing-using-metals/>. [Accessed 24 August 2015].
- [3] J. Beuth and N. Klingbeil, "The Role of Process Variables in Laser-Based Direct Metal Solid Freeform Fabrication," *JOM*, pp. 36-39, 2001.
- [4] J. Gockel, J. Beuth and K. Taminger, "Integrated control of solidification microstructure and melt pool dimensions in electron beam wire feed additive manufacturing of Ti-6Al-4V," *Additive Manufacturing*, Vols. 1-4, no. Inaugural, pp. 119-126, 2014.
- [5] J. Gockel, *Integrated Control of Solidification Microstructure and Melt Pool Dimensions In Additive Manufacturing Of Ti-6Al-4V*, Pittsburgh, PA: Carnegie Mellon University, 2014.

- [6] L. E. Murr, S. A. Quinones, S. M. Gaytan, M. I. Lopez, A. Rodela, E. Y. Martinez, D. H. Hernandez, E. Martinez, F. Medina and R. B. Wicker, "Microstructure and mechanical behavior of Ti-6Al-4V produced by rapid-layer manufacturing for biomedical applications," *Journal of the mechanical behavior of biomedical materials*, vol. 2, no. 1, pp. 20-32, 2009.
- [7] A. Safdar, *A Study on Electron Beam Melted Ti-6Al-4V*, Lund: Lund University, 2012.
- [8] N. Hrabe, R. Kircher and T. Quinn, "Effects of Processing on Microstructure and Mechanical Properties of Ti-6Al-4V Fabricated using Electron Beam Melting (EBM): Orientation and Location," in *Solid Freeform Fabrication*, Austin, 2012.
- [9] M. Donachie, *Titanium a technical guide*, ASM, 2007.
- [10] G. Lutjering and J. C. Williams, *Titanium*, Springer, 2007.
- [11] P. A. Kobryn and S. L. Semiatin, "Microstructure and texture evolution during solidification processing of Ti-6Al-4V," *Journal of Materials Processing Technology*, vol. 135, no. 2-3, pp. 330-339, 2003.
- [12] T. R. Mahale, *Electron Beam Melting of Advanced Materials and Structures, mass customization, mass personalization*, Raleigh, North Carolina: North Carolina State University, 2009.
- [13] J. C. Fox, *Transient Melt Pool Response in Additive Manufacturing of Ti-6Al-4V*, Pittsburgh, PA: Carnegie Mellon University, 2015.
- [14] ASTM Standard E112-13, *Standard test methods for determining average grain size*, West Conshohocken, PA: ASTM International, 2013.